Effect of Particle Size on Flow and Mixing in a Bladed Granular Mixer

Avik Sarkar
School of Mechanical Engineering, Purdue University, West Lafayette, IN 47907

Carl R. Wassgren
School of Mechanical Engineering, Purdue University, West Lafayette, IN 47907

Industrial and Physical Pharmacy (by courtesy), Purdue University, West Lafayette, IN 47907

DOI 10.1002/aic.14629
Published online October 8, 2014 in Wiley Online Library (wileyonlinelibrary.com)

A number of studies have modeled flow and mixing of granular materials using the discrete element method (DEM). In an attempt to reduce computational costs, many of these DEM studies model particles larger than the actual particle size without investigating the implications of this assumption. Using DEM, the influence of the modeled particle size on flow and mixing in a bladed granular mixer is studied. The predicted flow microdynamics, including mixing rates, are strongly dependent on the particle diameter. The effect of particle size on macroscopic advective flow also is significant, particularly for dilute flow regions. These results suggest that the influence of particle size needs to be taken into consideration when using larger particles in DEM mixing simulations. To guide scale-up efforts, particle-size-based scaling relationships for several key flow measurements are presented. © 2014 American Institute of Chemical Engineers *AIChE J*, 61: 46–57, 2015
Keywords: particulate flows, mixing, discrete element method, scale-up, diffusion

Introduction

Particulate flow and mixing in various blender designs have been extensively modeled using the discrete element method (DEM).[1–4] Since DEM is a computationally expensive technique, the number of particles that can be realistically simulated is limited. DEM models with $O(10^5)$ particles or fewer are typical, although a few studies have been able to reach $O(10^6)$ particles.[5] In reality, granular mixers may contain more than $O(10^9)$ particles, for a particle diameter of 100 μm.[6,7] Since meaningful DEM simulations with $O(10^9)$ particles are currently intractable, most studies implement particle sizes that are much larger than actual powder grains.

The goal of this work is to systematically investigate the influence of the particle size on advective flow (quantified by solid fraction, velocities, and torque) and microdynamic behavior (characterized by velocity distributions, coordination number, and diffusion coefficient). A periodic slice from a horizontal bladed mixer with rotating impeller blades is selected for this study, motivated by the geometry used in previous studies of a continuous granular mixer,[8–12] With a better understanding of particle size effects, scale-up relationships may be developed for this commonly used class of blenders.

Current affiliation of A. Sarkar: Process Modeling and Engineering Technology, Pfizer Inc., Groton, CT 06340
Correspondence concerning this article should be addressed to A. Sarkar at aviksarkar2@gmail.com.

Background

Bridgwater et al.[13] were some of the early researchers to identify that particle size affects the random diffusive particle motion in a granular bed agitated by a moving blade. They found that the advective horizontal displacements were independent of the particle size, but the displacements' standard deviations, a measure of mixing, was particle-size dependent. Bridgwater et al.[13] simply stated that this standard deviation of particle displacements will be a function of the particle diameter but did not propose one themselves.

Scott and Bridgwater[14] and Bridgwater[15] reported "self-diffusion" coefficients for spherical particles in a simple shearing apparatus. The self-diffusion coefficients were scaled by the square of the particle diameter (d_p^2). A more detailed relationship between the diffusion coefficient and particle diameter was referenced in Khakhar et al.[16] and Ottino and Khakhar,[17] and discussed in greater detail by Savage,[18] and is given by

$$D = f(\nu) d_p^2 \frac{dv_x}{dy}, \tag{1}$$

where D is the isotropic diffusion coefficient, $f(\nu)$ is a function of the solid fraction ν, and dv_x/dy is the shearing strain rate. Equation 1, however, does not account for the strong anisotropy existing in granular shear flows.[19] For shear flows, d_p^2-based scalings may be justified as the particle size is the only obvious length scale. An additional length scale is provided by the mixer dimensions D_{drum} for drum and bladed mixers, which is also likely to affect advective and diffusive particle motion.

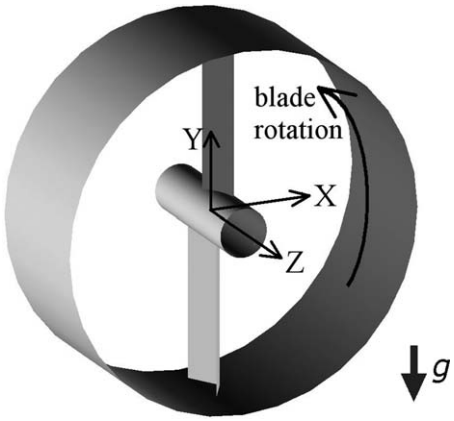

Figure 1. Schematic of the periodic slice mixer geometry.

Geometric aspect ratios are preserved for the cases where drum diameter is varied. The simulated device dimensions are summarized in Table 1. Gravity (g) acts vertically downwards in the view shown.

It is known that the advective flow in rotating drums is dependent on the particle size relative to the drum diameter. Khakhar et al.[16] and Orpe and Khakhar[20] showed that the thickness and shear rate in the active layer are dependent on the dimensionless size ratio $D_{\text{drum}}/d_{\text{p}}$. Additional evidence for the drum-size dependence on advective flow was obtained when the bed free surface shape[16,20] and streamwise velocities in the shearing layer[21] were also found to depend on $D_{\text{drum}}/d_{\text{p}}$. Alexander et al.[22] experimentally determined that the ratio of bed surface velocity to peripheral drum speed is proportional to $(D_{\text{drum}}/d_{\text{p}})^{1/6}$ for smaller rotation speeds (less than 30 rpm), and proportional to $(D_{\text{drum}}/d_{\text{p}})^{1/4}$ for larger speeds (greater than 30 rpm). It is apparent that the ratio $D_{\text{drum}}/d_{\text{p}}$ is a significant dimensionless quantity affecting particle flows in confined geometries.

These previously mentioned studies clearly establish that particle size affects advective and diffusive flow in rotating drum mixers. It remains to be seen whether these relationships between particle size and flow can be generalized to other granular mixers, or whether studies specific to the device of interest need to be performed.

Mixing simulations of a vertical axis, bladed mixer were performed by Radeke et al.[5] for varying dimensionless size ratios $D_{\text{drum}}/d_{\text{p}}$. The simulations reported in Radeke et al.[5] were performed for different dimensionless impeller rotation rates (or Froude numbers, defined in the Method section), and, therefore, a direct comparison of mixing rates is misleading. However, it was readily apparent that the simulations with smaller particles required more blade rotations to achieve a similar degree of homogeneity.

Experimental studies of mixing in a rotating drum were performed by Abouzeid et al.[23] Although they varied the particle size between 211 and 599 μm, this range was too small for them to notice any significant change in the residence time distribution, axial transport behavior, or bulk holdup. Studies by Pernenkil[24] of a double-helical ribbon blender showed that bigger particles yielded larger axial diffusion coefficients. Since only two particle sizes were investigated by Pernenkil,[24] their results can only be interpreted to identify qualitative differences in mixing rates as particle size changes.

Hassanpour et al.[25] investigated the influence of particle size in a twin axis, horizontal paddle mixer using DEM. They clearly showed that the predicted average particle speed increases linearly with simulated particle size. A similar particle-size dependence can be expected for other mixing devices that also operate on the principle of achieving agitation via rotating blades/paddles (such as the mixer that will be considered in this study, described in the Method section). No comparisons of mixing rates were performed in Hassanpour et al.[25]

The existing literature clearly establishes that both the macroscopic advective flow and microdynamic behavior depend on particle size, device size, and is specific to mixer geometry. A thorough systematic investigation of the effects of the simulated particle size on DEM flow simulations is lacking. In this study, this problem is addressed by simulating a section of a horizontal-axis bladed mixer, a common design for batch and continuous granular blenders.[6–12,26] The focus of this work is to better interpret the limitations of DEM predictions that arise from the use of larger particles. Particle-size-based scaling relations to improve DEM prediction accuracy are also presented.

Method

A periodic slice of a horizontal-axis mixer containing a pair of symmetric blades is used for this study (Figure 1). Two V-shaped impeller blades rotate with their convex side as the leading edge. This blade design is slightly different from previously used flat blades[8,9,11,12] to ensure that no macroscopic axial flow is produced. Hence, changes in flow or mixing behavior are solely due to varying particle size without interference from axial flow. The V-shape of the blades is expected to promote diffusive mixing and suppress coordinated advective flow in the transverse (X-Y) mixer plane. Mixer dimensions and geometry are summarized in Table 1. All simulations in this work are performed using an in-house, serial DEM code, which has been used in previous studies.[8–11]

Normal contact forces (F_{N}) are modeled by the Tsuji et al.[27] force model, comprised of a Hertzian spring with nonlinear damping, given by

$$F_N = k_{Hz}\delta^{3/2} + b_N\dot{\delta}\delta^{1/4}, \tag{2}$$

where k_{Hz} is the Hertzian contact stiffness and b_{N} is the normal damping coefficient, detailed in Sarkar and Wassgren[11] and Dubey et al.[12] This particular form of the normal force model was chosen as it yields a velocity-independent coefficient of restitution. Tangential forces are calculated using a

Table 1. Simulation Parameters

Parameter	Value(s)
Particle density	$\rho = 1000$ kg/m^3
Gravitational acceleration	$g = 9.81$ m/s^2
Drum diameter (baseline case[a])	$D_{\text{drum}} = 150$ mm
Axial periodic length	$L_{\text{per}}/D_{\text{drum}} = 0.4$
Shaft diameter	$D_{\text{shaft}}/D_{\text{drum}} = 0.1333$
Blade length	$l_{\text{blade}}/D_{\text{drum}} = 0.4333$
Blade width (each arm of V-shape)	$w_{\text{blade}}/D_{\text{drum}} = 0.1000$
Blade angle (between arms of V-shape)	120°
Young's modulus (particles and walls)	1 MPa
Poisson's ratio (particles and walls)	0.3
Normal restitution coefficient	0.5
Sliding friction coefficient (particle–particle and particle-wall)	0.3
Particle size, dimensionless[b]	$D_{\text{drum}}/d_{\text{p}} = 12.5$–$100$
Froude number (dimensionless impeller speed)	$Fr = 0.30$–1.06

[a]Additional simulations were performed for $D_{\text{drum}} = 75$, 112.5, and 225 mm. However, the ratio $D_{\text{drum}}/d_{\text{p}}$ was determined to be the key dimensionless number.
[b]For reference, the range of absolute particle sizes simulated are $d_{\text{p}} = 1.5$–12.0 mm.

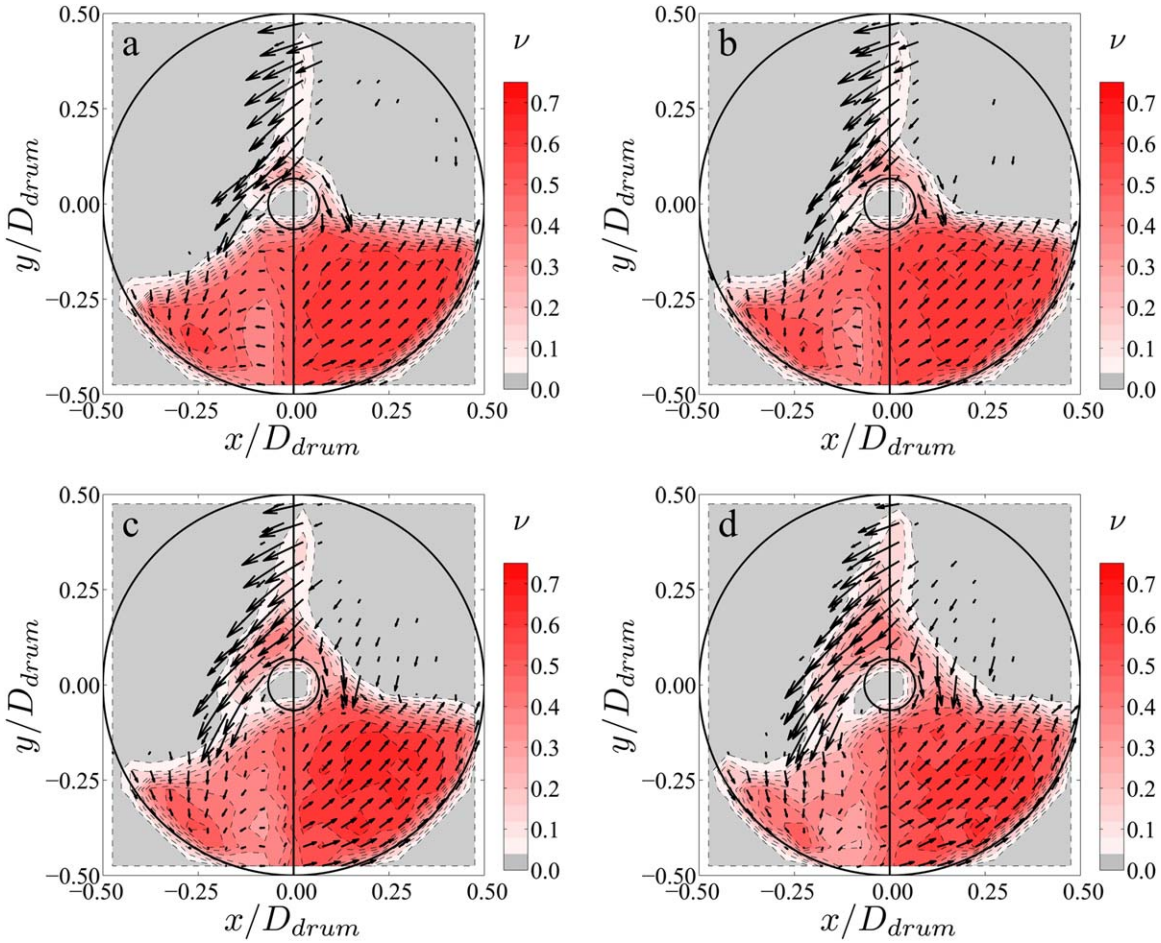

Figure 2. Averaged solid fraction and velocity vectors at $z/L_{per} \approx -0.28$, (a) $D_{drum}/d_p = 100$, (b) $D_{drum}/d_p = 75$, (c) $D_{drum}/d_p = 50$, and (d) $D_{drum}/d_p = 37.5$; presented for the representative $Fr = 0.84$ case.

Vertical lines show the orientation of impeller blades. [Color figure can be viewed in the online issue, which is available at wileyonlinelibrary.com.]

simple Coulomb friction model, given by $F_T = \mu_s F_N$, where F_T and F_N are the tangential and normal contact force magnitudes, respectively, and μ_s is the coefficient of sliding friction between the contacting surfaces. In agitated granular mixers, tangential interactions are dominated by sliding friction and the simpler Coulomb friction model is generally adequate; rolling friction is not included.

For an undamped Hertzian contact, the duration T_{bc} of an ideal binary collision between two identical particles with a characteristic impact speed $\omega D_{drum}/2$ is given by

$$T_{bc} \approx 3.36 \left[\frac{\rho^2 d_p^5 (1-\nu_P^2)^2}{\omega D_{drum} E^2} \right]^{1/5}, \quad (3)$$

where E and ν_P are the Young's modulus and Poisson's ratio, ω is the impeller rotation speed, and ρ is the particle density. Particles of all sizes are assumed to be made of the same material, and, therefore, the material properties E and ν are held constant (Table 1). Previous studies[28–30] have shown that averaged particle trajectory and velocity measurements, relevant to mixing studies, are relatively insensitive to the Young's modulus. As such, many DEM studies use particles with a smaller elastic modulus compared to real particles (see: Hassanpour et al.,[25] McCarthy et al.,[1] Sudah et al.,[3] to name just a few). This work also uses particles possessing greater pliability yet with stiffness sufficient for mixing simulations.

From Eq. 3, it is seen that the collision duration T_{bc} decreases with particle size, which, in turn, necessitates a smaller simulation time step Δt to accurately resolve a typical collision event. Simulations with smaller particle sizes are computationally more expensive not only due to the increased number of particles but also due to the need for smaller time steps. A value of $T_{bc}/\Delta t \approx 30$ is maintained for all d_p values in the present simulations, which is sufficiently small to accurately resolve particle trajectories during collisions.[31]

The effects of particle size on flow and mixing is studied by varying D_{drum}/d_p. This dimensionless size ratio can be varied by changing either d_p or D_{drum}. Although d_p is varied in the majority of the simulations, a few simulations with varying D_{drum} are also presented (refer to Table 1). It will be demonstrated that the dimensionless particle size D_{drum}/d_p is more important than the absolute values of d_p or D_{drum}. The scaling relationships developed are expressible as functions of D_{drum}/d_p.

The impeller rotation rate is expressed as the dimensionless Froude number Fr, given by

$$Fr = \frac{\omega^2 (D_{drum}/2)}{g}, \quad (4)$$

where ω is the blade rotation speed and g is the acceleration due to gravity. Several values of Froude number are investigated (Table 1), based on typical operating speeds of real mixers.[6,7] A particular case, $Fr = 0.84$, is studied more

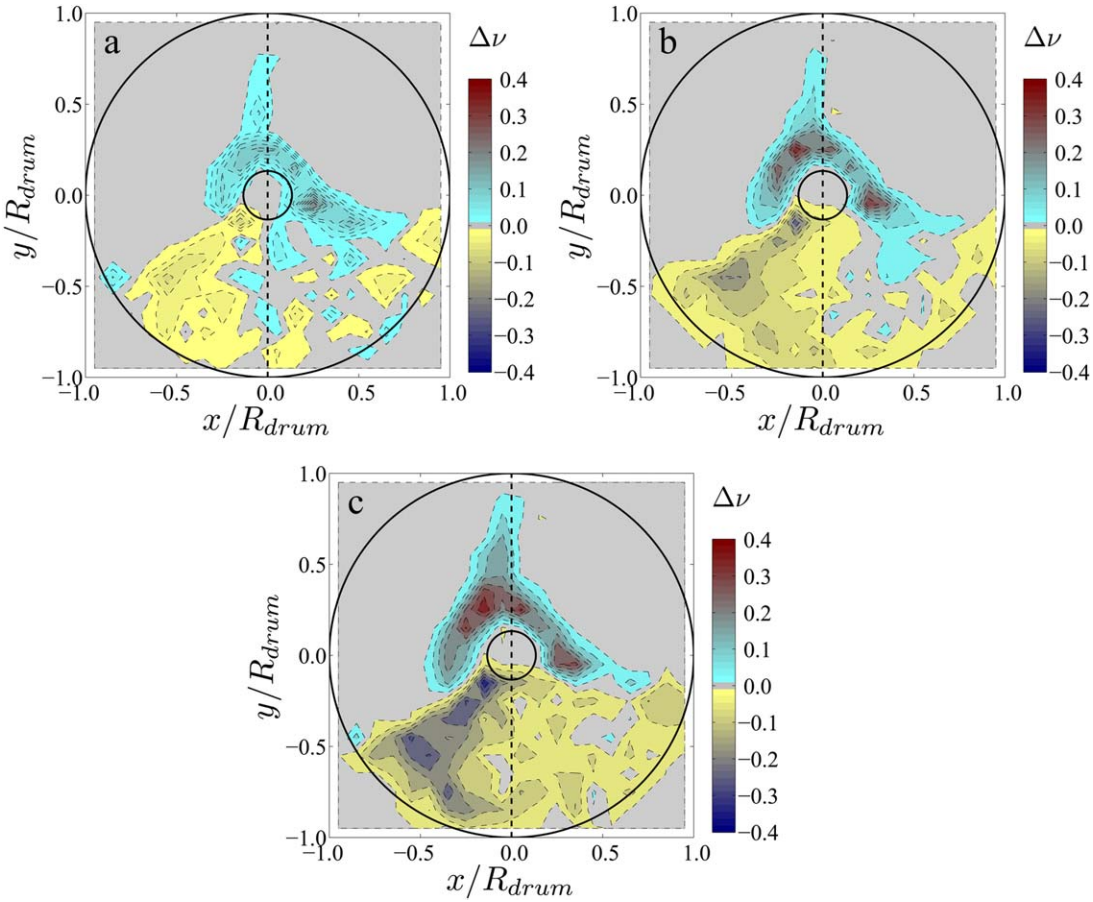

Figure 3. Differences in average local solid fraction ($\Delta\nu$) between the more-accurate $D_{drum}/d_p = 100$ case and (a) $D_{drum}/d_p = 75$, (b) $D_{drum}/d_p = 50$, (c) $D_{drum}/d_p = 37.5$ cases, presented for $Fr = 0.84$.

All contours plotted for the cross section at $z/L_{per} \approx -0.28$. Vertical dotted lines represent the orientation of impeller blades. [Color figure can be viewed in the online issue, which is available at wileyonlinelibrary.com.]

thoroughly—additional simulations are performed with smaller particle diameters. Many of the comparisons will be presented for this representative $Fr = 0.84$ case, but the results are equally valid for other impeller speeds.

The number of particles N_p in the simulations is given by

$$N_p = \frac{0.64\, v_{bulk} \cdot \frac{\pi}{4}(D_{drum}^2 - D_{shaft}^2)L_{per}}{\frac{\pi}{6} d_p^3}, \quad (5)$$

where D_{shaft} is the shaft diameter and L_{per} is the periodic length of the mixer slice. The factor 0.64 accounts for the voidage in a randomly packed bed of spheres. A bulk fill level of $v_{bulk} = 0.30$ is used for all simulations, based on experimental[6,7] and computational[11,12] measurements of typical holdups in bladed mixers. A uniform size distribution of $\pm 20\%$ the mean diameter d_p is assigned to the particles to prevent ordered crystalline packing.

It should be noted that the computational speed of DEM simulations scale nonlinearly with N_p, typically varying between $O(N_p)$ and $O(N_p^2)$, depending on software implementation. The smallest particle size that could be simulated in this work is $d_p = 1.50$ mm (corresponding to 113,152 particles), which is still larger than real powder particles ($d_p \sim 0.05$–0.5 mm). Nonetheless, valuable qualitative and quantitative insights regarding the influence of particle size are gained.

Cohesive and aerodynamic forces, which may become significant at smaller particle sizes,[32] are not considered in the current set of studies. At present, behavior of noncohesive particles is investigated and the choice of including cohesion is deferred to a future study.

Experimental validation of DEM results is not addressed in this study as previous validation studies have already demonstrated that DEM can accurately reproduce the flow of real noncohesive particles in bladed granular mixers (see, e.g., Remy et al.[33]). In this work, the well-established DEM technique is used to investigate the influence of particle size on flow and mixing.

Advective Flow and Impeller Torque

Local solid fraction and velocity values are calculated by subdividing the domain into cubical bins: 20, 20, and 8 bins are considered along the X, Y, and Z directions, respectively. For clarity, figures and detailed comparisons of advective flow fields and velocity profiles are presented only for the smaller particle size cases (D_{drum}/d_p ranging from 37.5 to 100). The smaller particles are closer in size to real particle diameters and, hence, are of greater interest.

After a few initial transient blade rotations, the bed behavior and averaged velocities exhibit periodically steady temporal profiles, indicating periodic steady-state flow has been achieved. From the steady-state measurements, instantaneous values of the mean solid fraction and mean particle velocity are recorded for all bins. For a given blade orientation, these measurements are then averaged over several blade rotations (≥ 8).

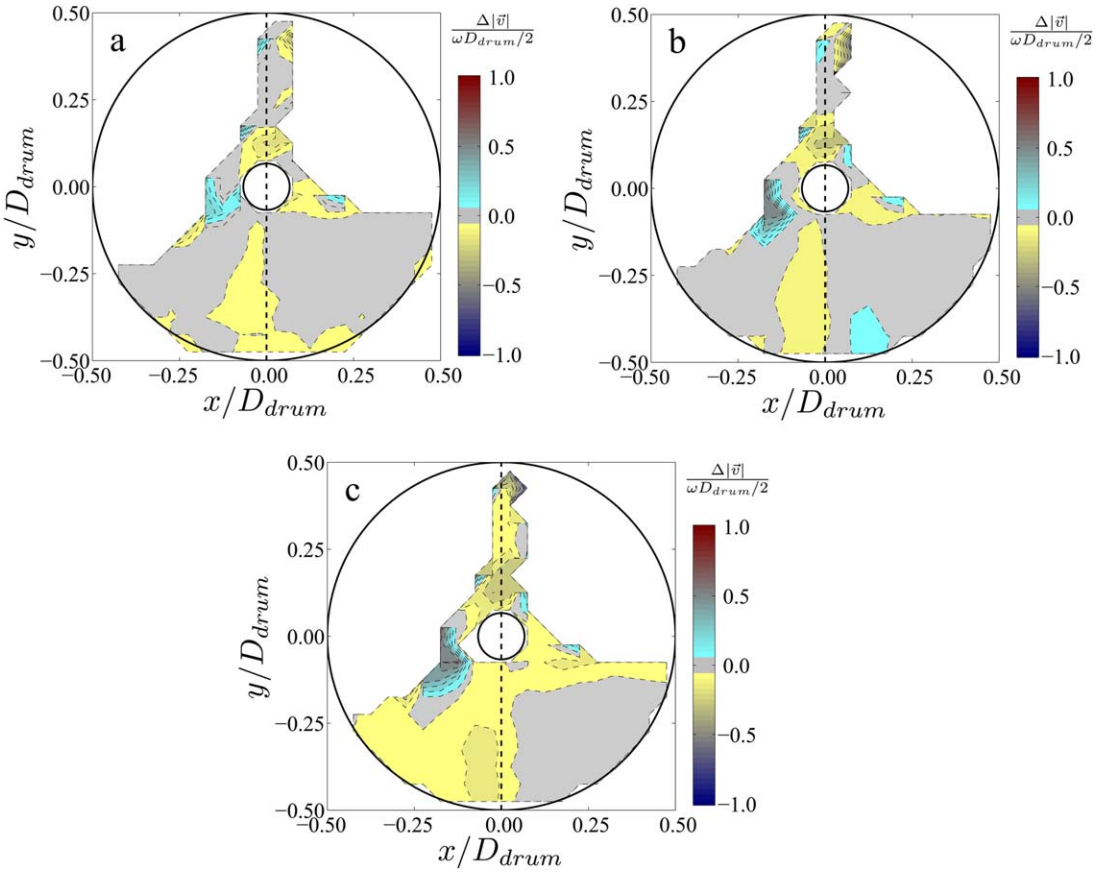

Figure 4. Differences in average local particle speed ($\Delta|\vec{v}|$) between the more-accurate $D_{drum}/d_p = 100$ case and (a) $D_{drum}/d_p = 75$, (b) $D_{drum}/d_p = 50$, (c) $D_{drum}/d_p = 37.5$ cases, presented for $Fr = 0.84$.

All contours are plotted for the cross section at $z/L_{per} \approx -0.28$. Vertical dotted lines represent the orientation of impeller blades. White areas denote the regions with insufficient particles to compute the average speed. [Color figure can be viewed in the online issue, which is available at wileyonlinelibrary.com.]

A comparison of these flow features for different particle sizes are shown for the cross sectional plane at $z/L_{per} \approx -0.28$ (Figure 2). The position of the impeller blades is indicated by vertical lines. The blades rotate counterclockwise in the view shown.

Similar bed behavior is exhibited by all particle size cases. Material upstream of the lower blade has the largest solid fraction because it is subjected to compressive forces by the counterclockwise-rotating blades. A region of larger voidage is observed in the wake of the rotating blades. Some particles are carried out of the bed by the blades and thrown over the central shaft. The bed shape does not vary much with changing particle size.

However, on closer examination, several differences in flow and packing emerge. As the particle size increases, the blades carry a larger volume of particles out of the bed. This increase in particle mass in the top half of the mixer is compensated by a decrease in solid fraction in the wake of the blade. For the larger particle size cases, speeds in the the top half of the mixer also appear to be larger.

In addition to describing the macroscopic flow differences qualitatively, the prediction errors associated with using larger particles should also be quantified. To make this quantitative comparison, the DEM simulation with the smallest particles ($D_{drum}/d_p = 100$) is considered to be a better representation of the real flow. The results of this smallest-particle-size case ($D_{drum}/d_p = 100$) are then subtracted from measurements of the large-particle cases ($D_{drum}/d_p = 37.5$, 50.0, and 75.0).

Figure 3 presents the relative differences in solid fraction, that is, the solid fractions reported in Figures 2b–d minus the smallest-particle solution ($D_{drum}/d_p = 100$) of Figure 2a. This relative difference illustrates the accuracy (or lack thereof) of large-particle DEM simulations compared to the $D_{drum}/d_p = 100$ case. Regions with negligible differences (less than 1% variation in solid fractions) are colored gray, which include large parts of the bed in front of the lower blade, that also happen to be the densely packed regions subject to compression. The largest differences are observed in the wake of the blade near the free surface and in the vicinity of the top blade—regions where solid fractions are small. Although the measured relative differences are larger throughout the bed for bigger simulated particles, the dilute regions exhibit greater discrepancies compared to denser regions of the flow.

A similar comparison of the relative differences in particle speed is presented in Figure 4. The speed differences are consistent with the solid fraction differences: predictions for the dilute regions (blade wake and above the shaft) are less accurate compared to the dense regions (front of the blade). Juxtaposition of Figure 2 against Figures 3 and 4 reveals a clear correlation between the difference predictions and local solid fraction. Based on this observation, the following hypothesis is proposed: DEM simulations with larger

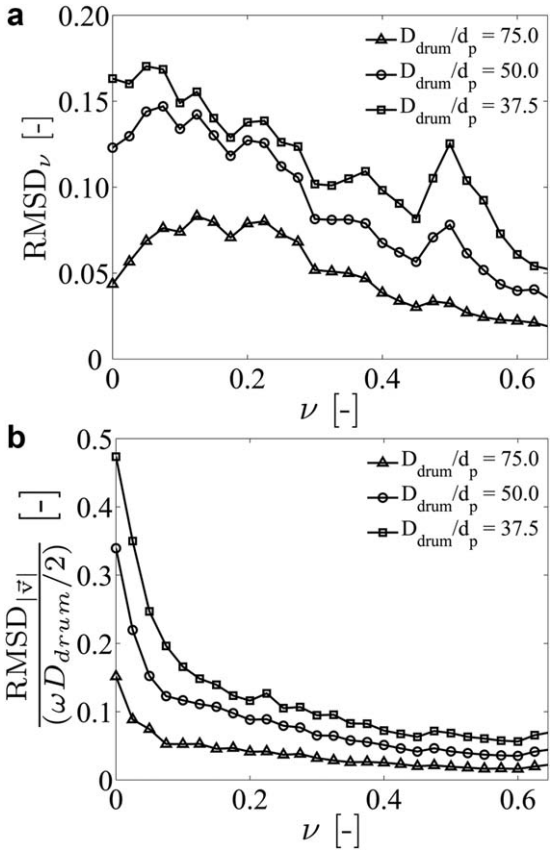

Figure 5. Root mean square difference (dimensionless) for (a) solid fraction $RMSD_\nu$, and (b) average particle speed $RMSD_{|\vec{v}|}$, between the smallest particle size case ($D_{drum}/d_p = 100$) and larger particle size simulations ($D_{drum}/d_p = 37.5$, 50, 75) as a function of local solid fraction ν.

Each data point is a measure of the local error in the region with corresponding local solid fraction ν. The errors are shown for the representative $Fr = 0.84$ case.

particles yield better predictions for dense regions, but are less accurate for dilute regions. Simulating larger particle sizes to obtain advective behavior may be acceptable for predominantly dense systems (e.g., rotating drum mixers) but is a poor choice for dilute flows.

To test the aforementioned hypothesis, the root mean square difference (RMSD) for solid fraction and speed are calculated as a function of the local solid fraction ν (Figure 5). The $RMSD_\nu$ value for a solid fraction value ν is defined as

$$RMSD_\nu = \langle (v_{large} - v_{small})^2 \rangle^{1/2}, \quad (6)$$

where angular brackets $\langle \cdot \rangle$ denote an average of the enclosed statistics collected from regions with local solid fraction ν. The difference $v_{large} - v_{small}$ represents the error between the larger particle size cases ($D_{drum}/d_p = 37.5$, 50.0, or 75.0) and the smallest-particle solution ($D_{drum}/d_p = 100$). The $RMSD_{|\vec{v}|}$ values are similarly calculated by substituting v_{large} and v_{small} in Eq. 6 with $|\vec{v}|_{large}$ and $|\vec{v}|_{small}$, respectively.

The proposed hypothesis is confirmed by the results presented in Figure 5. For a given particle size case, $RMSD_\nu$ values generally decrease with increasing local solid fraction ν. (Local peaks at $\nu \approx 0.5$ are observed for the $D_{drum}/d_p = 50$ and 37.5 cases, but their origin could not be determined.) Furthermore, $RMSD_{|\vec{v}|}$ values increase monotonically with decreasing ν, and are considerably larger at small solid fractions (Figure 5b). Both $RMSD_\nu$ and $RMSD_{|\vec{v}|}$ values increase systematically as the diameter difference between the larger simulated particles and the more-accurate $D_{drum}/d_p = 100$ case increases. Based on these results, it can be confidently concluded that flow predictions are more sensitive to D_{drum}/d_p in dilute regions but less so in dense regions.

To ascertain that larger particles can indeed yield reasonably good predictions in the denser flow regions (compared to the more accurate, small-particle simulation), a representative densely packed volume of the bed is examined (Figure 6a). Particles in this volume are subject to compression by the rotating blades, resulting in larger local solid fractions. Varying the simulated particle diameter does not produce any appreciable differences in the axial solid fraction profile (Figure 6b). A comparison of the axial speed distributions (Figure 6c) further shows that the predictions in this dense region are insensitive to the simulated particle size. Examination of other densely packed regions directly above the volume marked in Figure 6a also show no noticeable dependence on the simulated particle size (not presented separately as figures). Therefore, for predominantly dense flows, use of larger particles is a reasonable approximation for DEM models when advective flow is of interest. This finding is consistent with the experimental studies of Bridgwater et al.[13] involving flow past a single mixing blade, where advective particle displacements were found to be independent of d_p.

The last advective flow quantity investigated is the average impeller torque ($\bar{\Gamma}_z$) required to rotate the blades through the bed. The torque relates to the work done on the particles by the blades and, therefore, to the degree of agitation the material experiences. The time-averaged impeller torque is calculated using

$$\bar{\Gamma}_z = \frac{1}{T_{rot}} \sum_{\substack{\text{all time steps} \\ \text{during } T_{rot}}} \sum_{\substack{\text{all} \\ \text{contacts}}} \left[\vec{r}_c(t) \times \vec{F}_c(t) \right] \cdot \left[-\hat{k} \right] \Delta t, \quad (7)$$

where $\vec{r}_c$ and $\vec{F}_c$ are the instantaneous location and force vectors for a particle-blade contact (in the blade's frame of reference), and $\hat{k}$ is the unit vector along the shaft axis. The inner summation computes the net instantaneous impeller torque due to all particle-blade contacts. The outer summation yields the time-averaged torque over one impeller rotation. Equation 7 provides the correct approach to accurately compute the torque. The contact forces must be sampled and averaged every time step Δt, otherwise a significant number of particle-blade collision events may be mistakenly ignored.

The $\bar{\Gamma}_z$ measurements, made dimensionless by a characteristic torque scale $\rho D_{drum}^5 \omega^2$, are presented as a function of D_{drum}/d_p (Figure 7a). First, the suitability of D_{drum}/d_p for the purposes of developing scaling laws must be evaluated. It remains to be seen whether D_{drum}/d_p is the meaningful dimensionless number, or if the two length scales D_{drum} and d_p need to be considered separately. For the $Fr = 0.84$ case, two approaches to adjust D_{drum}/d_p were adopted: d_p was varied while holding D_{drum} constant, and vice versa. Both approaches yield almost identical values for the dimensionless torque (and other measurements presented later). Therefore, D_{drum}/d_p is the appropriate dimensionless parameter for scaling relationships; absolute values of d_p or D_{drum} are unimportant.

The dimensionless torque measurements for different impeller rotation speeds can be collapsed to a single curve by a simple Froude number scaling (Figure 7b), given by

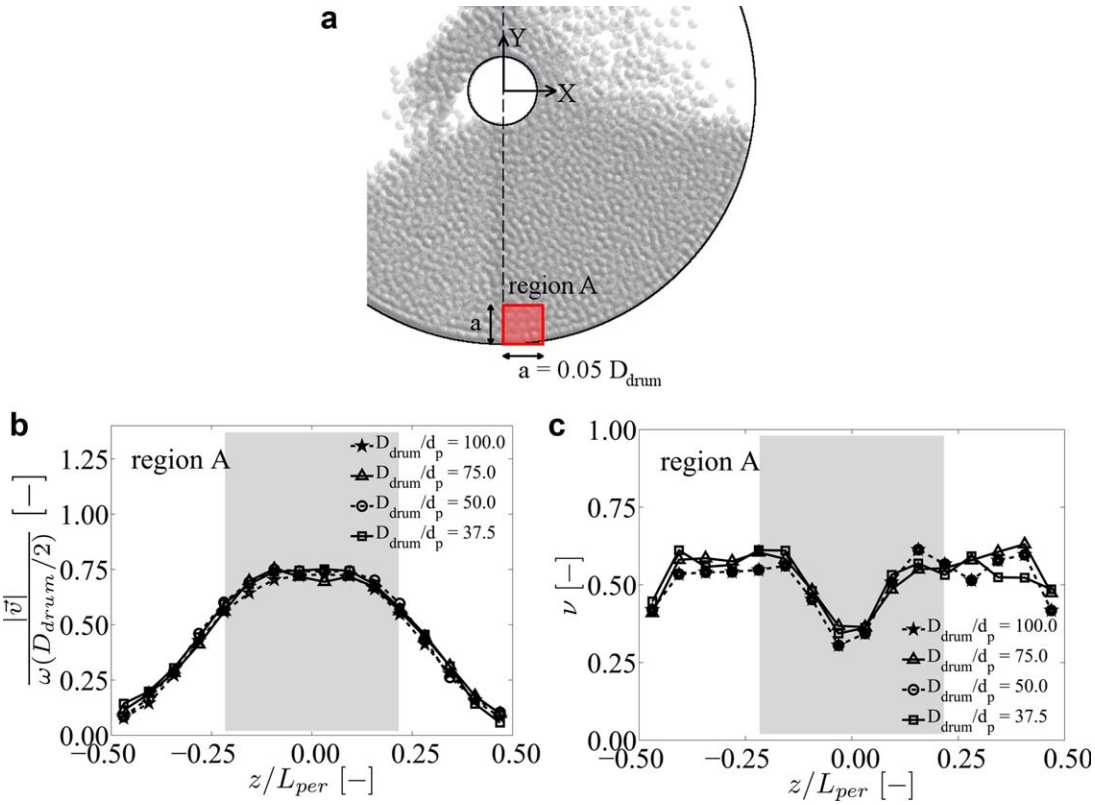

Figure 6. Comparison of the axial (*Z*) distribution of solid fraction and particle speed for varying D_{drum}/d_p in a dense flow region of the bed.

(a) Location of the dense region "A", (b) solid fraction in region A, and (c) average speed in region A. Shaded regions in (b) and (c) mark the projected axial extents of the blades. [Color figure can be viewed in the online issue, which is available at wileyonlinelibrary.com.]

$$\frac{\bar{\Gamma}_z}{(\rho D_{\text{drum}}^5 \omega^2)} \approx Fr^{-0.9}\left[0.002601 + 0.001677e^{-0.04305\frac{D_{\text{drum}}}{d_p}}\right]. \quad (8)$$

The impeller torque, made dimensionless and scaled thus, is found to decrease with increasing D_{drum}/d_p, and eventually asymptotes for infinitesimally small particles (or infinitely large mixers). Larger particles in DEM simulations overestimate the torque, but the $D_{\text{drum}}/d_p = 100$ case prediction is within 2% of the asymptotic value (extrapolated for cohesionless particles without air effects).

Velocity and Speed Distributions

It was previously demonstrated that particle speed prediction errors increase with the size of simulated particles. The flow microdynamics is probed further by constructing frequency distributions of particle speeds and velocity components (Figure 8). Particle velocities over 10 impeller rotations with 48 regularly spaced blade orientations (per rotation) are included to determine these frequency distributions.

Bimodal curves for particle speed distributions are obtained for all particle sizes (Figure 8a). The first mode occurs at a value close to zero, representing the almost-motionless particles that are able to settle in between blade passes. Note that there is no contribution from dead zones as the entire bed experiences some degree of agitation (refer to Figure 6c). The proportion of almost-motionless particles increases with decreasing particle size, consistent with the findings of Hassanpour et al.[25] In this study, there is a significant change in the proportion of nearly static particles as d_p is varied. The percentage of particles with speeds less than 0.05 times the blade tip speed increases from 5.8% for the $D_{\text{drum}}/d_p = 12.5$ case to 21.0% for $D_{\text{drum}}/d_p = 100$ ($Fr = 0.84$). This change in the fraction of almost-stationary particles is expected to impact mixing behavior; the mixing rates should decrease with particle size.

The secondary peak in Figure 8a represents the modal speed of the agitated particles, which varies with particle size—larger speeds are observed for larger particles. The frequency distributions for velocity components v_x, v_y, and v_z also are constructed (Figures 8b–d). The distribution of v_z is symmetric around $v_z = 0$, as expected, given the axial symmetry in blade design. Asymmetric distributions for v_x and v_y are obtained because particle agitation occurs mainly in the transverse (X-Y) plane. Consistent with the $f(|\vec{v}|)$ results, $f(v_x)$, $f(v_y)$, and $f(v_z)$ distributions also exhibit a systematic dependence on D_{drum}/d_p. The bed microdynamics are clearly affected by the simulated particle size.

There is an overprediction of the velocity magnitudes when larger particles are simulated (Figure 8). The average speed (nondimensionalized) of all particles in the bed is found to vary linearly with d_p/D_{drum} (Figure 9a). A velocity correction can be developed based on this linear trend. First, the data points for different impeller speeds are collapsed to a line by a Froude-number-based scaling (Figure 9b), given by

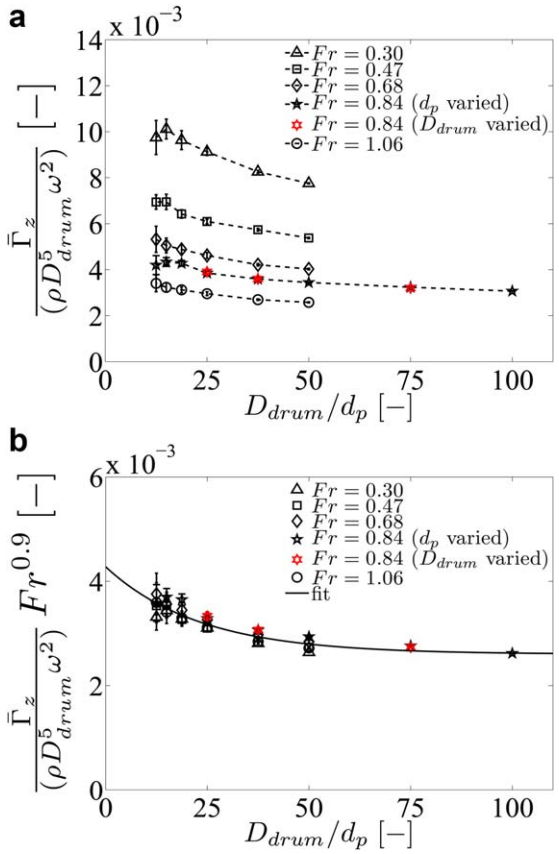

Figure 7. Torque experienced by the impeller blades for varying D_{drum}/d_p and *Fr*, (a) made dimensionless by $\rho D_{drum}^5 \omega^2$ and (b) further scaled using *Fr*.

Scatter bars represent plus/minus one standard deviation of the average torque recorded over several impeller rotations. [Color figure can be viewed in the online issue, which is available at wileyonlinelibrary.com.]

$$\frac{|\overrightarrow{v}|_{\text{average}}}{\omega(D_{\text{drum}}/2)} \approx Fr^{0.15}\left[0.2028+4.375\frac{d_p}{D_{\text{drum}}}\right], \qquad (9)$$

where $|\overrightarrow{v}|_{\text{average}}$ is the bed-averaged particle speed. Then, velocity predictions from large-particle DEM simulations can be scaled down to the appropriate d_p value by a factor determined from Eq. 9. Strictly speaking, the velocity correction should also be a function of the local solid fraction ν, as it was shown that speed errors depend on ν as well (Figure 5b). At present, the solid-fraction dependence is ignored and it is suggested, as a first engineering approximation, that the same correction factor be applied throughout the bed. Note that the dimensionless number D_{drum}/d_p (or, rather, its reciprocal) appears in the scaling law for particle speed (Eq. 9), as was the case for torque (Eq. 8, Figure 7); individual values of d_p and D_{drum} are unimportant.

Hassanpour et al.[25] also report a similar linear relationship between the mean speed and particle size for their bladed paddle blender. Their attempts to use this relationship to extraploate the speed of real particles, experimentally measured using position emission particle tomography, did not yield satisfactory results. Idealization of the particle shapes in DEM models was blamed for the discrepancy between simulations and experiments. The authors of this present work think that emergence of secondary physical effects, such as cohesion and fluid effects for actual powder particles, could also be a source of error. Extrapolation of the scaling expressions, derived using noncohesive DEM simulations, is valid only if the underlying physics remain unchanged, i.e., actual powder particles are also cohesionless (e.g., in this work, even the smallest particle size cases obey the trends shown in Figures 7 and 9). If additional physics are important to the problem, they should be incorporated in the DEM models employed for scale-up studies.

Coordination Number and Diffusion Coefficient

The coordination number is another convenient and useful measurement for characterizing the microscopic flow and packing structure of a granular bed (Figure 10). The mean particle–particle coordination number c_{pp} is calculated using a time-averaging scheme similar to the torque calculation method (Eq. 7): coordination number statistics are sampled and averaged after every time step Δt for all particles. The particle-boundary contacts are not included in this computation.

In the absence of wall effects, that is, for infinitely large beds and/or infinitesimally small particles, the coordination number should be independent of the particle size. However, in bounded vessels such as the present mixer, wall effects can be significant and the mean c_{pp} is a function of D_{drum}/d_p. As the particle size decreases, the contribution to c_{pp} from the near-wall region declines compared to the contribution from bed interior. The value of c_{pp} eventually approaches an asymptotic limit c_∞ for infinitesimally small particles ($D_{\text{drum}}/d_p \to \infty$). This asymptotic value c_∞ is of interest for real particles.

A simple model is proposed to describe the relationship between c_{pp}, d_p, and D_{drum} (see Appendix for details). This model considers the contributions to coordination number from the bed's interior and near-wall regions, and expresses c_{pp} as a fraction of c_∞, given by

$$c_{pp} \approx c_\infty \frac{1+\psi_1\left(\frac{d_p}{D_{\text{drum}}}\right)}{1+\psi_2\left(\frac{d_p}{D_{\text{drum}}}\right)}, \qquad (10)$$

where ψ_1 (≈ 8.443) and ψ_2 (≈ 43.61) are geometry-dependent fitting parameters with values satisfying the requirements described in the Appendix. The asymptotic coordination number value (c_∞) depends on the impeller speed.[8] A simple Froude number scaling captures this dependence for the present mixer: $c_\infty \approx 5.11 Fr^{-0.28}$. The model given by Eq. 10 fits the data well. For example, the intermittently agitated bed at $Fr = 0.84$ yields a reasonable value of $c_\infty = 5.37$ (compare with 5.5–6.4 for stationary packed beds[34]). The ratio D_{drum}/d_p continues to be the key dimensionless quantity for scaling coordination number, consistent with the findings for torque and speed (Figures 7 and 9).

The predicted c_{pp} values are considerably smaller than the c_∞ value even for simulations with $D_{\text{drum}}/d_p = 100$. If the bed microstructure is of interest, modeling larger particles in DEM simulations is a poor approximation. In such scenarios, coordination-number corrections must be developed and applied.

The time-averaged particle-blade coordination number c_{pb} was also computed (not separately presented as a figure). The number of particle-blade contacts should relate to the blade area ($\propto D_{\text{drum}}^2$) and the projected particle surface area ($\propto d_p^2$). After scaling, the quantity $c_{pb} d_p^2 / D_{\text{drum}}^2$ is found to be almost almost

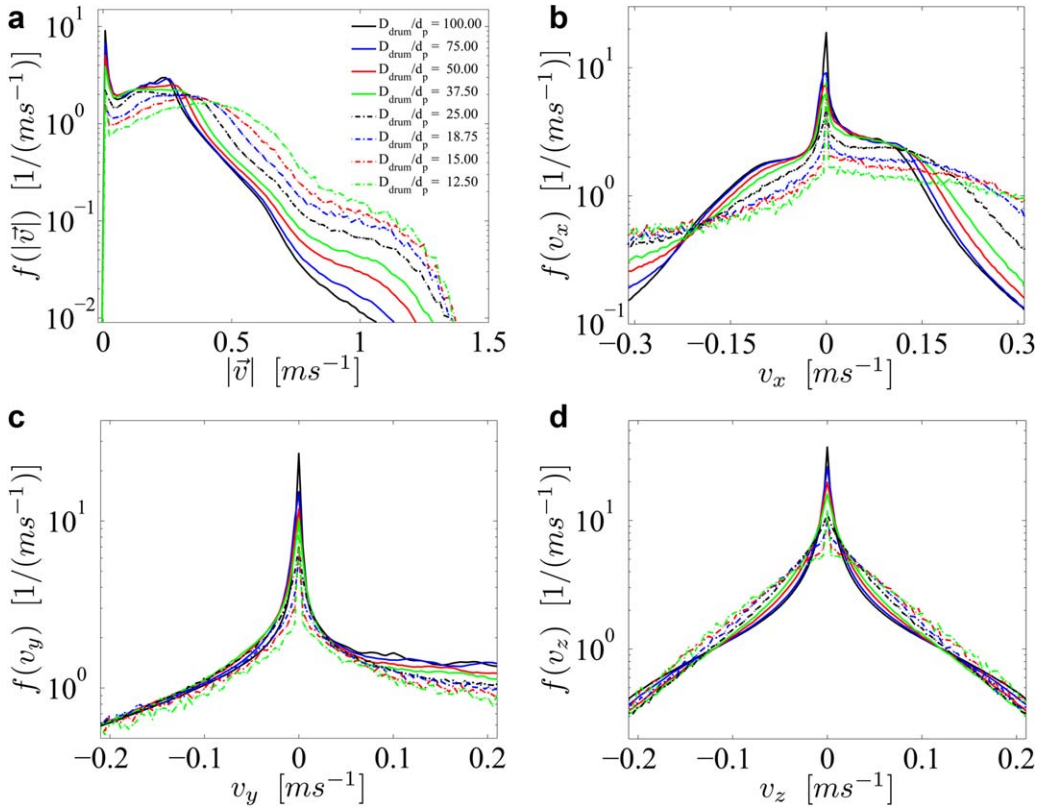

Figure 8. Frequency distribution functions for particle speed and velocity components for varying particle size, (a) speed $f(|\vec{v}|)$, and velocity components (b) $f(v_x)$, (c) $f(v_y)$, (d) $f(v_z)$.

Note the logarithmic scales of the *Y*-axes. Distribution functions are shown for the representative $Fr = 0.84$ case. [Color figure can be viewed in the online issue, which is available at wileyonlinelibrary.com.]

constant for a given Fr value. This result provides a measure for the number of particles (c_{pb}) agitated by the blades through direct contact, and thus a method for evaluating blade efficacy.

Finally, the effect of particle size on mixing rates is studied. Granular diffusion coefficients, also referred to as "self-diffusion coefficeints," have been commonly used to measure granular mixing rates.[12,19,35] Commonly encountered measures of mixing that are based on artificially tagging particles as separate species (such as relative standard deviation) are not used here. The measurements from such an approach depend on how the species are initially tagged (e.g., top/bottom, side/side, front/back). The diffusion approach eliminates this dependence on initial conditions.

The granular diffusion coefficients are expressed by the symmetric tensor, D_{ij}. For diffusion processes obeying Fick's law, D_{ij} is calculated as

$$D_{ij} = \lim_{t\to\infty} \frac{\langle \Delta x_i(t) \Delta x_j(t) \rangle}{2t}, \tag{11}$$

where $\Delta x_i(t)$ is the random diffusive displacement of a particle in the i^{th} direction ($i, j = X, Y, Z$) at time t, obtained after subtracting any contribution from mean advective flow. The angular brackets $\langle \cdot \rangle$ indicate an instantaneous average of the expression within, over all particles in the domain. The limit $t \to \infty$ is used to attenuate initial transients, though in practice a sufficiently large time serves the same purpose.

The first step towards determining the D_{ij} values is to ascertain whether the granular diffusion process obeys Fick's law. Mixing along the mixer axis (Z) shows the characteristics of Fickian diffusion: linear variations of $\langle \Delta z \Delta z \rangle$ with time are observed for all cases (Figure 11 shows a representative case). The axial diffusion coefficient is easily calculated from the slope of this line, which is $2D_{zz}$ (Eq. 11). However, the diffusion process in this mixer is anisotropic, demonstrated by Campbell[19] to be a common feature of granular flows.

Mixing in the transverse directions (X and Y) is clearly non-Fickian, further complicated by the presence of physical walls that bound the values of $\langle \Delta x \Delta x \rangle$ and $\langle \Delta y \Delta y \rangle$. (Periodic boundaries imply the mixer is unbounded along the Z-direction.) The D_{xx} and D_{yy} values could not be reliably determined from the present data, but it can be inferred that transverse mixing is much faster than axial mixing. The off-diagonal terms in the D_{ij} tensor were also examined but were found to be relatively small.

The computed D_{zz} values, made dimensionless by ωD_{drum}^2, can be used to characterize the influence of particle size on mixing rates (Figure 12). The dimensionless diffusion coefficients vs. d_p/D_{drum} data collapse on a straight line, without the need for Froude number scaling (although ω appears in the nondimensionalization). A scaling relationship for D_{zz} is given by

$$\frac{D_{zz}}{(\omega D_{drum}^2)} \approx k\left(\frac{d_p}{D_{drum}}\right), \tag{12}$$

where k is the only fitting parameter, determined to be 0.01355 for the present mixer geometry. This linear variation of the diffusion coefficient with d_p is a departure from the previously reported d_p^2 dependence.[14–18] Moreover, Eq. 12

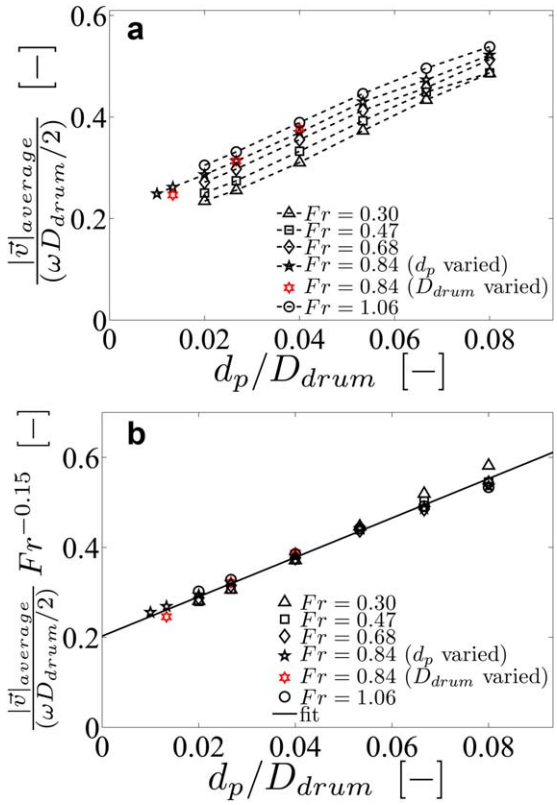

Figure 9. Average particle speed for varying d_p/D_{drum} and *Fr*, (a) made dimensionless by blade tip speed ($\omega D_{drum}/2$) and (b) further scaled using *Fr*.

[Color figure can be viewed in the online issue, which is available at wileyonlinelibrary.com.]

shows that $D_{zz} \propto D_{drum}$, that is, the device length scale is also important in bladed mixers. This dependence on D_{drum} can possibly be linked to the blade size (which scales with D_{drum}). More particles are agitated by a larger blade, thus increasing the diffusion coefficient.

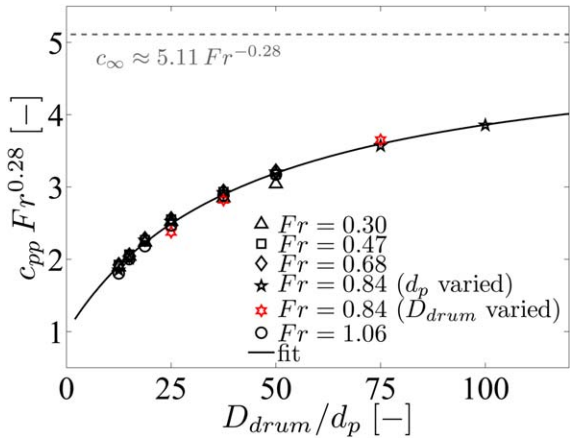

Figure 10. Particle–particle coordination number, scaled using *Fr*, for varying D_{drum}/d_p and *Fr*.

Solid and dotted lines show the fit and asymptotic limit, respectively, given by Eq. 10. [Color figure can be viewed in the online issue, which is available at wileyonlinelibrary.com.]

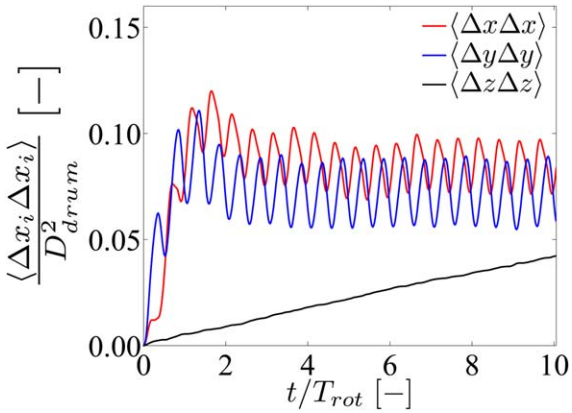

Figure 11. Mean square random displacements, made dimensionless by D_{drum}^2, as a function of the number of impeller rotations (t/T_{rot}).

Arepresentative case for $D_{drum}/d_p = 37.5$ and $Fr = 0.84$ is shown, but all cases exhibit similar behavior. [Color figure can be viewed in the online issue, which is available at wileyonlinelibrary.com.]

Equation 12 may be used to extrapolate the diffusion coefficients for smaller particles, assuming the underlying physics remain unchanged. The granular mixing rates are significantly overpredicted by using larger particles in DEM studies. Notwithstanding, Eq. 12 provides a convenient starting point for developing particle-diameter-based corrections for DEM predictions, which then can be used to estimate mixing rates more accurately for smaller particles.

Conclusions

DEM simulations are used to demonstrate the effects of the modeled particle size, which are often larger than actual particles, on flow and microdynamics in a bladed granular mixer. Quantitative scaling relationships based on the dimensionless particle size (D_{drum}/d_p) and impeller speed (Fr) are presented for several key flow measurements. These relationships can be used to understand the influence of particle-size

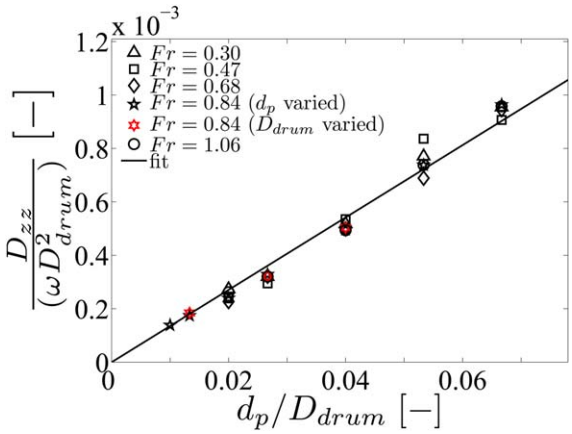

Figure 12. Axial diffusion coefficients D_{zz}, made dimensionless by ωD_{drum}^2, for varying d_p/D_{drum} and *Fr*.

The solid line is the fit given by Eq. 12. [Color figure can be viewed in the online issue, which is available at wileyonlinelibrary.com.]

assumptions on DEM results, and, thus, better utilize the predictions from large-particle DEM simulations.

Although the advective flow patterns appear similar, the average speed and distribution of velocity components are functions of D_{drum}/d_p. The dependence on D_{drum}/d_p is strongest at smaller solid fractions, suggesting that the use of larger particles in DEM models may be a poor approximation for predicting the advective flow in predominantly dilute systems. Furthermore, the flow microdynamics depend strongly on the particle size for dilute as well as dense flows. For example, the diffusion coefficient D_{zz} in the present granular mixer is found to be a linear function of the particle diameter d_p. DEM simulations with larger particles will tend to overpredict the degree of mixing, assuming the particle physics remain unchanged as particle size decreases. The scaling laws presented in this work provide perspective on the particle size effects in DEM simulations and may be used to develop quantitative corrections for the large-particle results.

The methodology presented in this work can serve as a basis for addressing scale-up of a wide class of powder mixers and granular unit operations. However, cohesion and air effects should be included when developing more realistic scale-up models. Additional factors, such as actual particle-size distributions and friction, should also be considered in future studies. Although this study is limited to grains with a narrow size range, the particle-size distribution may become important in certain applications where the powders have broad distributions.

DEM simulations of commercial mixers with realistic particle sizes remain outside the reach of current computational resources, but particle-size-based scaling relationships are a viable alternative for accurately predicting real powder flow. Validation of scaling laws, including extrapolation of the relationships presented in this work, remains to be addressed, subject to availability of detailed experimental data or computational resources that can afford fine-particle simulations (for instance, parallelized GPU-based DEM codes, Radeke et al.[5]).

Acknowledgment

The authors acknowledge the support of the National Science Foundation Engineering Research Center for Structured Organic Particulate Systems (NSF ERC-SOPS, EEC-0540855).

Literature Cited

1. McCarthy JJ, Khakhar DV, Ottino JM. Computational studies of granular mixing. *Powder Technol.* 2000;109(1–3):72–82.
2. Bertrand F, Leclaire LA, Levecque G. DEM-based models for the mixing of granular materials. *Chem Eng Sci.* 2005;60(8–9):2517–2531.
3. Sudah OS, Arratia PE, Alexander A, Muzzio FJ. Simulation and experiments of mixing and segregation in a tote blender. *AIChE J.* 2005;51(3):836–844.
4. Chaudhuri B, Mehrotra A, Muzzio FJ, Tomassone MS. Cohesive effects in powder mixing in a tumbling blender. *Powder Technol.* 2006;165(2):105–114.
5. Radeke CA, Glasser BJ, Khinast JG. Large-scale powder mixer simulations using massively parallel GPU architectures. *Chem Eng Sci.* 2010;65(24):6435–6442.
6. Portillo PM, Ierapetritou MG, Muzzio FJ. Characterization of continuous convective powder mixing processes. *Powder Technol.* 2008;182(3):368–378.
7. Vanarase AU, Muzzio FJ. Effect of operating conditions and design parameters in a continuous powder mixer. *Powder Technol.* 2011;208(1):26–36.
8. Sarkar A, Wassgren CR. Simulation of a continuous granular mixer: effect of operating conditions on flow and mixing. *Chem Eng Sci.* 2009;64(11):2672–2682.
9. Sarkar A, Wassgren C. Continuous blending of cohesive granular material. *Chem Eng Sci.* 2010;65(21):5687–5698.
10. Sarkar A. *Modeling a Continuous Granular Mixer Using Periodic Discrete Element Method Sub-Models.* PhD thesis, Purdue University, 2011.
11. Sarkar A, Wassgren C. Comparison of flow microdynamics for a continuous granular mixer with predictions from periodic slice DEM simulations. *Powder Technol.* 2012;221:325–336.
12. Dubey A, Sarkar A, Ierapetritou M, Wassgren CR, Muzzio FJ. Computational approaches for studying the granular dynamics of continuous blending processes, 1 DEM based methods. *Macromol Mater Eng.* 2011;296(3–4):290–307.
13. Bridgwater J, Bagster DF, Chen SF, Hallam JH. Geometric and dynamic similarity in particle mixing. *Powder Technol.* 1969;2(4):198–206.
14. Scott AM, Bridgwater J. Self-diffusion of spherical particles in a simple shear apparatus. *Powder Technol.* 1976;14(1):177–183.
15. Bridgwater. J. Self-diffusion coefficients in deforming powders. *Powder Technol.* 1980;25(1):129–131.
16. Khakhar DV, McCarthy JJ, Gilchrist JF, Ottino JM. Chaotic mixing of granular materials in two-dimensional tumbling mixers. *Chaos.* 1999;9(1):195–205.
17. Ottino JM, Khakhar DV. Mixing and segregation of granular materials. *Annu Rev Fluid Mech.* 2000;32(1):55–91.
18. Savage SB. Disorder, diffusion and structure formation in granular flow. In. Bideau D, Hansen A, editors. *Disorder and Granular Media*, North Holland, 1993:255–285.
19. Campbell CS. Self-diffusion in granular shear flows. *J Fluid Mech.* 1997;348:85–101.
20. Orpe AV, Khakhar DV. Scaling relations for granular flow in quasi-two-dimensional rotating cylinders. *Phys Rev E.* 2001;64(3):031302.
21. Jain N, Ottino JM, Lueptow RM. An experimental study of the flowing granular layer in a rotating tumbler. *Phys Fluids.* 2002;14(2):572–582.
22. Alexander A, Shinbrot T, Muzzio FJ. Scaling surface velocities in rotating cylinders as a function of vessel radius, rotation rate, and particle size. *Powder Technol.* 2002;126(2):174–190.
23. Abouzeid AZMA, Mika TS, Sastry KV, Fuerstenau DW. The influence of operating variables on the residence time distribution for material transport in a continuous rotary drum. *Powder Technol.* 1974;10(6):273–288.
24. Pernenkil L. *Continuous Blending of Dry Pharmaceutical Powders.* PhD thesis, Massachusetts Institute of Technology, 2008.
25. Hassanpour A, Tan H, Bayly A, Gopalkrishnan P, Ng B, Ghadiri M. Analysis of particle motion in a paddle mixer using discrete element method (DEM). *Powder Technol.* 2011;206(1–2):189–194.
26. Laurent BFC, Bridgwater J. Performance of single and six-bladed powder mixers. *Chem Eng Sci.* 2002;57(10):1695–1709.
27. Tsuji Y, Tanaka T, Ishida T. Lagrangian numerical simulation of plug flow of cohesionless particles in a horizontal pipe. *Powder Technol.* 1992;71(3):239–250.
28. Yuu S, Abe T, Saitoh T, Umekage T. Three-dimensional numerical simulation of the motion of particles discharging from a rectangular hopper using distinct element method and comparison with experimental data (effects of time steps and material properties). *Adv Powder Technol.* 1995;6(4):259–269.
29. Kuo HP, Knight PC, Parker DJ, Adams MJ, Seville JPK. Discrete element simulations of a high-shear mixer. *Adv Powder Technol.* 2004;15(3):297–309.
30. Freireich B, Litster J, Wassgren C. Using the discrete element method to predict collision-scale behavior: a sensitivity analysis. *Chem Eng Sci.* 2009;64(15):3407–3416.
31. Cundall PA, Strack ODL. A discrete numerical model for granular assemblies. *Geotechnique.* 1979; 29(1):47–65.
32. Chowhan ZT, Linn E.E. Mixing of pharmaceutical solids. I. Effect of particle size on mixing in cylindrical shear and V-shaped tumbling mixers. *Powder Technol.* 1979;24(2):237–244.
33. Remy B, Canty TM, Khinast JG, Glasser BJ. Experiments and simulations of cohesionless particles with varying roughness in a bladed mixer. *Chem Eng Sci.* 2010;65(16):4557–4571.
34. Powell MJ. Computer-simulated random packing of spheres. *Powder Technol.* 1980;25(1):45–52.
35. Natarajan VVR, Hunt ML, Taylor ED. Local measurements of velocity fluctuations and diffusion coefficients for a granular material flow. *J Fluid Mech.* 1995;304:1–25.

Appendix: Mean Particle-Particle Coordination Number

The packing in the interior of a granular bed is generally different than the packing near boundary walls or the free surface (Figure A1). For a nonsegregated particle assembly, the particle–particle coordination number near the boundaries is generally smaller than that in the interior of the bed due to differences in packing. In a vessel of finite size, these differences in packing affect the bed-averaged particle–particle coordination number c_{pp}. As particle size decreases, the influence of the wall regions on the average c_{pp} value diminishes. In this Appendix, a simple analytical model is presented to account for the effect of boundaries on average particle–particle coordination number.

Let the particle–particle coordination number for a bed of infinitesimally small particles be c_∞, which is also the coordination number in the core region of the bed away from boundaries. For regions near the boundaries (i.e., region 1, region 2, etc. in Figure A1), let the coordination number be c_1, c_2, etc. The number of particles in the interior region of the bed N_{int} is given by

$$N_{int} = \frac{v_{int} V_{int}}{v_p}, \tag{A1}$$

where v_{int} and V_{int} are the solid fraction and total volume of the interior region, and v_p is the (characteristic) particle volume. The number of particles N_i in region i ($i = 1, 2, \ldots$) is given by

$$N_i = \frac{v_i V_i}{v_p}, \tag{A2}$$

where v_i and V_i are the solid fraction and total volume of boundary region i.

The average particle–particle coordination number for the entire bed is the weighted average of the coordination numbers in each region, the weights being the number of particles in each region, given by

$$\begin{aligned} c_{pp} &= \frac{N_{int} c_\infty + (N_1 c_1 + N_2 c_2 + \cdots)}{N_{int} + (N_1 + N_2 + \cdots)} \\ &= \frac{\frac{v_{int} V_{int}}{v_p} c_\infty + \left(\frac{v_1 V_1}{v_p} c_1 + \frac{v_2 V_2}{v_p} c_2 + \cdots \right)}{\frac{v_{int} V_{int}}{v_p} + \left(\frac{v_1 V_1}{v_p} + \frac{v_2 V_2}{v_p} + \cdots \right)} \\ &= \frac{c_\infty + \left(\frac{v_1 V_1}{v_{int} V_{int}} c_1 + \frac{v_2 V_2}{v_{int} V_{int}} c_2 + \cdots \right)}{1 + \left(\frac{v_1 V_1}{v_{int} V_{int}} + \frac{v_2 V_2}{v_{int} V_{int}} + \cdots \right)}. \end{aligned} \tag{A3}$$

Usually, the influence of the boundaries is felt up to a depth of a few particle diameters normal to the boundaries. Hence, the boundary region volume $V_i \propto D^2 d_p$, where D^2 scales with the area of the boundary region (D being a characteristic vessel length scale) and d_p scales with the boundary region's depth. The interior volume of the bed can be approximated by $V_{int} \propto D^3$ (for sufficiently large vessels). Thus, the ratio of volume V_i to the volume of the interior V_{int}, appearing in Eq. A3, may be expressed as

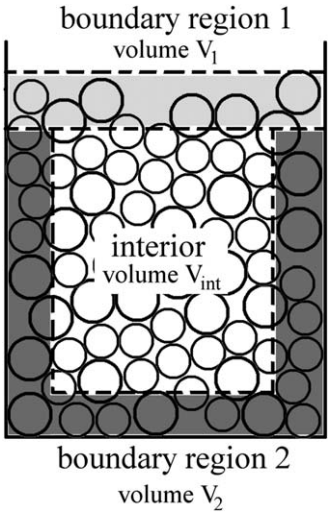

Figure A1. Idealized representation of a particle bed showing near-wall and interior regions with different packings.

$$\frac{V_i}{V_{int}} = k_i \frac{D^2 d_p}{D^3} = k_i \frac{d_p}{D}, \tag{A4}$$

where k_i values are system-boundary-dependent proportionality constants.

Substituting Eq. A4 into Eq. A3, the average particle–particle coordination number may be rearranged and written as

$$\begin{aligned} c_{pp} &= \frac{c_\infty + \left(\frac{v_1}{v_{int}} k_1 c_1 + \frac{v_2}{v_{int}} k_2 c_2 + \cdots \right) \frac{d_p}{D}}{1 + \left(\frac{v_1}{v_{int}} k_1 + \frac{v_2}{v_{int}} k_2 + \cdots \right) \frac{d_p}{D}} \\ &= c_\infty \frac{1 + \psi_1 \left(\frac{d_p}{D} \right)}{1 + \psi_2 \left(\frac{d_p}{D} \right)}, \end{aligned} \tag{A5}$$

where ψ_1 and ψ_2 are given by

$$\psi_1 = \frac{v_1}{v_{int}} k_1 \frac{c_1}{c_\infty} + \frac{v_2}{v_{int}} k_2 \frac{c_2}{c_\infty} + \cdots, \tag{A6}$$

$$\psi_2 = \frac{v_1}{v_{int}} k_1 + \frac{v_2}{v_{int}} k_2 + \cdots. \tag{A7}$$

Equation A5 provides an expression for the average particle–particle coordination number as a function of dimensionless particle size D/d_p (or its reciprocal), based on a simple model that recognizes the differences in packing between boundary and interior regions of the bed. From Eqs. A6 and A7, it can be expected that ψ_1 and ψ_2 depend primarily on the system geometry. From Eqs. A5—A7, it is apparent that fitted values for c_∞, ψ_1, and ψ_2 should yield positive, real numbers. In the limit $D/d_p \to \infty$ (i.e., infinitesimally small particles), the boundaries do not affect the mean coordination number, as expected, and $c_{pp} \to c_\infty$.

Manuscript received May 1, 2014, and revision received July 26, 2014.